Personal Dead Reckoning System with Shoe Mounted Inertial Sensors

SUJATHA RAJAGOPAL

KTH Electrical Engineering

Master's Degree Project
Stockholm, Sweden 2008

XR-EE-SB 2008:013

Abstract

User demands on tracking technologies supersedes the capabilities in several areas. Consumers desire accurate position, regardless of the environmental variation. The Global Positioning System (GPS) receivers on the market today do not live up to the demands.

This report proposes a method for indoor navigation. The method has been tested with simulated data and real world data. The system is useful for monitoring the position of emergency personnel inside buildings, where the GPS is unavailable. The proposed method, the Personal Dead-Reckoning (PDR) system with aid of the step detector uses a 3-axis Inertial Measurement Unit (IMU) attached to the user's boot. Step detector detects the stance phases of a walking event. Stance phase detection is made to introduce zero velocity update (ZUPT) and zero angular rate update (ZARU), which reduce the errors of the PDR system. The IMU provide the angular rate and the acceleration of the foot, which are fed to the Inertial Navigation Equations (INS). The continuous-time navigation equations are derived in the tangent-frame (t-frame). An Extended Kalman Filter (EKF) for closed loop integration between the IMU measurements, the step detector and the INS is derived. The filter propagates and estimates the errors during the stance phase, which are fed back to the INS for correction of the internal navigation states.

Acknowledgements

I am grateful for being given the opportunity to do my Master thesis about Inertial Navigation System at Signal Processing Department of Royal Institute of Technology (KTH). I would like to thank all who have encouraged and helped me during my thesis work. Specifically, I would like to thank Professor Peter Händel, PhD students Isaac Skog and John-Olof Nilsson who have supported me during the project. The data filtering technique has been inspired by Isaac Skog's previous research in Inertial Navigation System. The hardware components of the system have been chose by Isaac Skoog. The study was financed by the Signal Processing Department of Royal Institute of Technology.

Contents

Chapter 1

Introduction

1.1 Background

It can be important to know the position of an object on Earth. Global Positioning System (GPS) has been developed for outdoor application such as navigation or geodetic measurements. GPS receivers are today the dominating positioning technique for positioning of both vehicles and individuals. With expensive equipment, it is possible to determine ones position on the Earths surface as accurate as a few centimeters. However, consumer grade receivers have an accuracy in the order of 15-100 m. Tracking method based solely on GPS is vulnerable, is expected to malfunction in indoor environments and challenging electromagnetic environments. The GPS signals can not be reached indoor because of the signal attenuation caused by the walls and the signals can be disordered and demodulated in the time at the electromagnetic environments. However, in environments and scenarios encountered by incident responders and military personnel the performance requirements can not be met by GPS only. Therefore, some other alternative techniques to GPS exist. Some of them are local-radio based positioning system, dead-reckoning and inertial navigation systems.

A multiple of different local radio-based positioning systems exist, some of them are Ultra-Wideband (UWB) system and Wireless local Area Networks (WLAN) system [1]. The local radio-based techniques are mainly developed to improve the navigation performance of an area of short range. Wireless UWB positioning techniques can provide real time indoor and outdoor precision tracking. UWB transmitters are positioned in known locations inside a room. They estimate the distances to all other stationary transmitters. The characteristics of UWB signals provide the position and location estimation. WLAN positioning system can use an existing infrastructure consisting of WLAN base stations which are present for wireless communication purposes. There are different techniques to allow WLAN positioning. One of them is received signal strength positioning. The base stations can estimate received signal strength (RSS) from mobile terminal. These RSS estimates from several base stations can be used to calculate the position of mobile terminal. WLAN positioning allows high accuracy if there is a base station in range of 10 m, otherwise the accuracy is highly dependent of the signal quality.

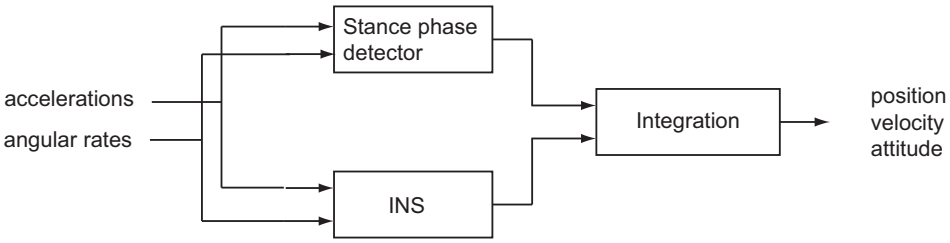

Figure 1.1: *A schematic description of the proposed system with its input and output signals.*

Another alternative to the GPS system is the dead reckoning (DR) system, which is the process of estimating user's current position based upon the previously determined position and the acceleration and the angular velocity. The main limitation with DR systems when using as a stand-alone system is that the error growth is unbounded. However, the error can, if sufficiently accurate sensors are combined with intelligent signal processing, be small during shorter time interval. An inertial navigation system (INS) builds upon the DR principle. INS is based on measurements from three-axis sensors including accelerometers and gyros, the sensors are called Inertial Measurement Unit (IMU).

Step detection, of a walking person, and Extended Kalman Filter (EKF) in combination with DR, gives a method for achieving positional information of the walking person. This method fulfills the users' requirements on accuracy and availability of the positioning service [2]. With shoe-mounted sensors it is possible to achieve the position error growth of a few percent. The proposed navigation system is described in Figure 1.1.

Positioning system for a walking person has many advantages, it does not require GPS, beacons or landmarks. The system is therefore useful in GPS-denied environments, such as inside buildings, tunnels and dense forests. The main disadvantage of the system is that the error grows rapidly with the time. In order to reduce the most significant errors caused by the bias drift of the accelerometers, an implementation of techniques known as Zero Velocity Update (ZUPT) and Zero Angular Update (ZARU) are introduced in combination with step detection. With the ZUPT and ZARU techniques and related signal processing algorithms, typical positional errors of the system are about 5 % of distance travelled for short walks [1].

1.2 Purpose of the thesis

This report will focus on developing a cheap and robust personnel navigation system [2] for positioning of emergency personnel in rescue operations. Personal navigation system is important for many users such as rescue services, fire brigades, police forces, military and other public services of high importance. It is possible to save many lives in future rescue operations by developing a robust personnel positioning system with high accuracy and availability. Robust tracking techniques have the potential to increase rescue personnel safety in many critical operation scenarios such as flooding, earth quakes, tropical storms and terrorist attacks. The system enable efficient control of operations which results

in increased possibility for secure operation [1].

The area of use is at GPS denied environments, such as indoor environments. The goal is to achieve good navigation for approximately 30 seconds. A navigation software package was available for GPS aided INS and the software was modified during the project. A step detector was added to the software package.

1.3 Thesis outline

The thesis is divided into 7 chapters:

- Chapter 2 presents the coordinate frame used in the thesis followed by the derivation of the coordinate transformation matrix from the body coordinate system to the tangent coordinate system.
- Chapter 3 reviews the basic principles used in the stance phase detector. It starts with a description of the error growth without the detector, followed by introducing the statical property of the stance phase.
- The ZUPT, the ZARU and the INS integration is described in Chapter 4. First a description of the Kalman Filter is presented followed by a description of the Extended Kalman Filter.
- In Chapter 5, the hardware involved in this project is described.
- The results are presented in Chapter 6. First, the result from simulated data is presented followed by the result from the real world data.
- Chapter 7 contains conclusions, provides suggestions for future development of the system.

The main contributions in this thesis are:

- Development of the stance phase detector.
- Modify existing EKF in MATLAB to the proposed navigation system.
- The proposed system is tested with the simulated and the real world data.

1.4 System Overview

There are a lot of works which have been presented about the integration between the INS and the step detector with aid of the ZUPT and ZARU techniques and the author would like to highlight two of them, which are closely related to the content of the thesis. Firstly, the paper [3] which describes the EKF for tracking with shoe mounted inertial sensors. Secondly, the report [4], where they have implemented similar system and presenting the simulation result on the paper.

A schematic description of the inertial navigation system with aid of ZUPT and ZARU in combination with the step detector is presented in Figure 1.2. The INS is the major navigation system. Stand alone INS system can provide errors which are unbounded in a few millisecond. In order to stabilize the system, the

step detector with ZUPT and ZARU techniques is introduced, which results in online calibration every half second.

Coordinate transformation is part of the implementation. The IMU data must be transformed into a common coordinate system, suitable for the integration. There are two frames used in the thesis, the tangent-frame and the body-frame. The tangent-frame, which is also called the t-frame has North, East and Down direction in an arbitrary point on the earth. The accelerations and the angular rates are measured with respect to the body frame (b-frame), which is the frame that is rigidly attached to the user's foot. In this project t-frame, [2], is used as the navigation-frame.

When the transformation of the coordinate systems is introduced for the IMU data, the data is then used with the inertial navigation equations to calculate the position, the velocity and the heading. The step detector is built upon the accelerometer and gyroscope measurements in b-frame, is used to composite the EKF filter during the stance phase. During the time instance when the foot is stationary, the EKF corrects the velocity errors and the gyro biases. The accelerometer biases and the attitude errors (roll and pitch) are observable in linear combination. The position errors and the yaw heading are the only EKF states that are not observable [3].

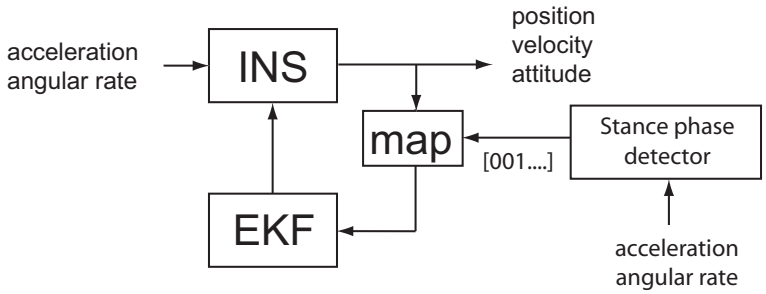

Figure 1.2: *Loosely coupled closed loop implementation of a ZUPT and ZARU aided inertial navigation system. EKF denotes the extended Kalman filter. The map part of the integration decides when to apply ZUPT and ZARU techniques.*

Chapter 2

Coordinate systems and transformations

Inertial Navigation System requires transformation of measured and computed quantities between various frames of reference. In the scope of this thesis there are two frames, the tangent frame (t-frame) which is the navigation frame and the body frame (b-frame) which is the frame used by IMU. Our system uses the standard strapdown inertial navigation system mechanization. The INS navigation is performed relative to the fixed tangent frame. Typically this integration need following stages.

1. The accelerometer and the gyro use the b-frame inside the IMU. First the heading information is updated with integration of the measured angular rates from the b-frame. Then the coordinate transformation matrix is calculated.
2. The b-frame accelerations are transformed to calculate the t-frame accelerations by using the transformation matrix.
3. The t-frame accelerations are integrated to calculate the t-frame velocity and position.

The relationship between the coordinate frames is given by the coordinate rotation matrix $\mathbf{R}_b^t$ which is a 3×3 matrix. In this chapter some of the necessary coordinate frames for the thesis are defined and a derivation necessary to transform between the reference frames are presented.

2.1 Coordinate Frame Definition

This section defines the different coordinate frames and corresponding notation used in this thesis. All coordinate systems are right-hand Cartesian systems, [2].

2.1.1 Tangent plane (t-frame)

The tangent plane is also called local geodetic plane. The tangent plane has the north, east and down direction. The tangent plane is attached to a fixed point on

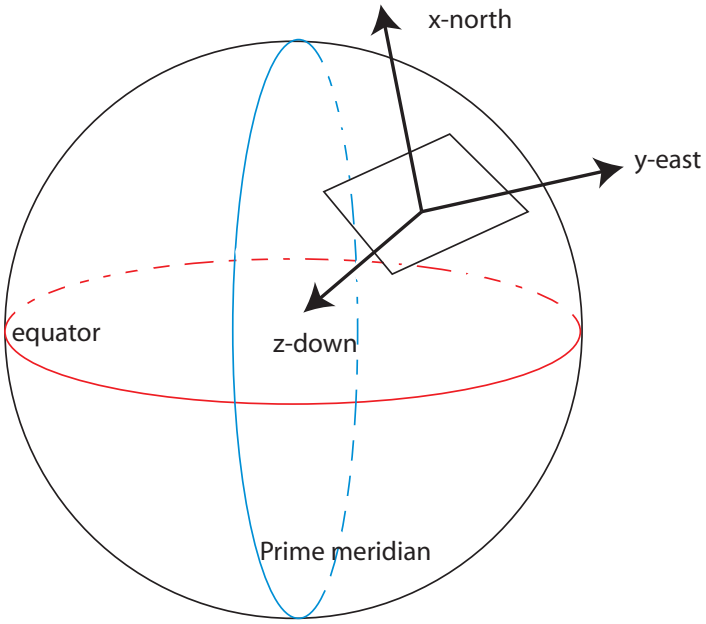

Figure 2.1: *Tangent-plane reference coordinate system.*

the surface of the earth at some convenient point for local measurements. This point is the origin of the local frame. The x-axis points north, y-axis points east and the z-axis completes the right-handed coordinate system pointing toward that interior of the earth perpendicular to the reference ellipsoid. The tangent plane is the navigation frame in this thesis work.

2.1.2 Body frame (b-frame)

The Body frame is sometime called vehicle frame. In our navigation application, the objectives is to determine the position of the user based on the measurements from the sensor platform attached to the user, see Figure 2.2

The body frame is rigidly attached to the user's boot. The x-axis is defined in the forward direction, the z-axis is defined to pointing to the bottom of the user's foot and y-axis completes the right-handed orthogonal coordinate system.

2.2 Coordinate Frame Transformation

As discussed earlier in this chapter, in a navigation system it is often necessary to transform a vector from one coordinate system into another coordinate system. In the project there is need for one transformation from body frame to tangent

Figure 2.2: *Body coordinate system.*

frame, as mentioned earlier. The following subsection describes the body to the tangent plane transformations, which is used in the thesis work.

2.2.1 Body to tangent frame transformations

Consider the typical situation illustrated in the Figure 2.3, which depicts two coordinate systems. The first one is the tangent frame coordinate system, which has its origin where the user has started to walk. The second frame is the body frame, which is rigidly attached to the user's shoe. The relationship between the body frame to the tangent frame coordinate systems can be completely described by the position $[x_b, y_b, z_b]^T$ of the body frame, the origin of the tangent frame and the orientation of coordinate frame.

In order to perform the transformation from the body frame to the tangent frame, it is necessary to introduce the rotation matrix between these frames. Rotation matrix can be defined by a series of three plane rotations involving Euler-angles (ϕ, θ, ψ), defined as (roll, pitch, yaw).

The first rotation is about the z-axis, which is rotated by ψ radians. This rotation aligns the new x'-axis with the projection of the body x_b-axis into the tangent plane, see Figure 2.1. The frame rotation is given by

$$\begin{bmatrix} x' \\ y' \\ z' \end{bmatrix} = \begin{bmatrix} \cos(\psi) & \sin(\psi) & 0 \\ -\sin(\psi) & \cos(\psi) & 0 \\ 0 & 0 & 1 \end{bmatrix} \begin{bmatrix} x_t \\ y_t \\ z_t \end{bmatrix} \tag{2.1}$$

Next rotation rotates the coordinate system by θ radians about the y'-axis. The rotation aligns the new x"-axis with the body x-axis. For this operation the frame rotation is described as

$$\begin{bmatrix} x'' \\ y'' \\ z'' \end{bmatrix} = \begin{bmatrix} \cos(\theta) & 0 & -\sin(\theta) \\ 0 & 1 & 0 \\ \sin(\theta) & 0 & \cos(\theta) \end{bmatrix} \begin{bmatrix} x' \\ y' \\ z' \end{bmatrix} \tag{2.2}$$

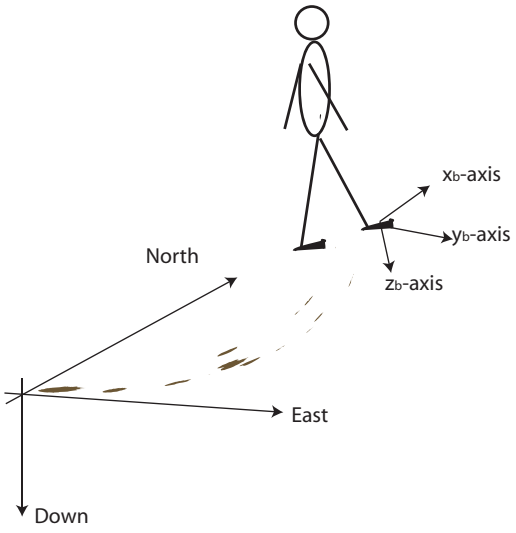

Figure 2.3: *An illustration of tangent frame and body frame during a walking scenario.*

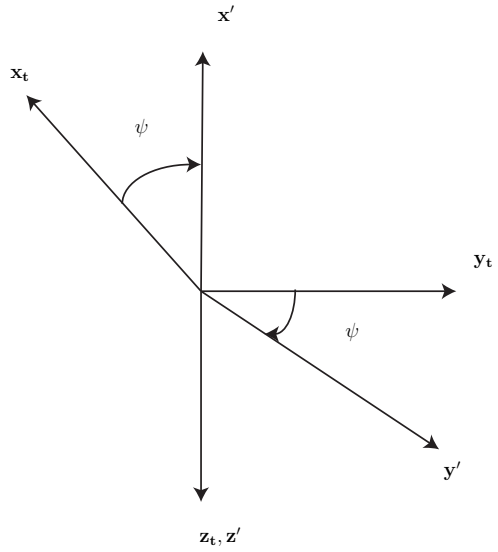

Figure 2.4: *Rotation 1.*

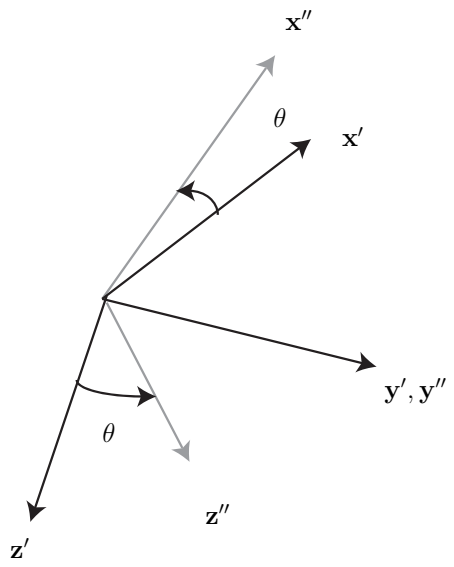

Figure 2.5: *Rotation 2.*

The third rotation is performed about x"-axis by ϕ radians. This rotations aligns the new axes with the body y_b and z_b axis. The frame rotation for this operation is described as

$$\begin{bmatrix} x_b \\ y_b \\ z_b \end{bmatrix} = \begin{bmatrix} x''' \\ y''' \\ z''' \end{bmatrix} = \begin{bmatrix} 1 & 0 & 0 \\ 0 & \cos(\phi) & \sin(\phi) \\ 0 & -\sin(\phi) & \cos(\phi) \end{bmatrix} \begin{bmatrix} x'' \\ y'' \\ z'' \end{bmatrix} \tag{2.3}$$

In this way the tangent frame coordinates can be transformed to the body frame coordinates by three rotations. The rotation matrix R_{t2b} can be found be multiplying all three rotations

$$\mathbf{R}_{t2b} = \tag{2.4}$$
$$\begin{bmatrix} c(\psi)c(\theta) & s(\psi)c(\theta) & -s(\phi) \\ -s(\psi)c(\phi) + c(\psi)s(\theta)s(\phi) & c(\psi)c(\phi) + s(\psi)s(\theta)s(\phi) & c(\theta)s(\theta) \\ s(\psi)s(\phi) + c(\psi)s(\theta)c(\phi) & -c(\psi)s(\phi) + s(\psi)s(\theta)c(\phi) & c(\theta)c(\theta) \end{bmatrix}$$

where the c and s stand for cosine and sine function.

$$\mathbf{v}_b = \mathbf{R}_{t2b}\mathbf{v}_t \tag{2.5}$$

$$\mathbf{R}_{t2b}^{-1}\mathbf{v}_b = \mathbf{R}_{t2b}^{-1}\mathbf{R}_{t2b}\mathbf{v}_t \tag{2.6}$$

$$\mathbf{R}_{t2b}^{-1} = \mathbf{R}_{t2b}^{T} \tag{2.7}$$

$$\mathbf{v}_t = \mathbf{R}_{t2b}^{T}\mathbf{v}_b \tag{2.8}$$

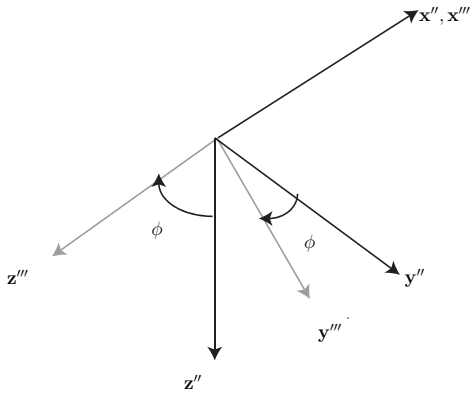

Figure 2.6: *Rotation 3.*

The transformed R_{t2b} gives the body to tangent plane matrix, R_{b2t}, since R_{t2b} is an unitary matrix.

Chapter 3

Detection of the footfall

In this chapter a description of the footfall event detection is presented, that is a detector which decides when to apply the ZUPT and the ZARU techniques. In order to detect the walking event, an Inertial Measurement Unit (IMU) is mounted on a foot. When the user walks, their feet alternate between a stationary stance phase and a moving stride phase. The detector detects the stance phase event and sends the information to the Extended Kalman Filter (EKF). EKF applies the ZUPT and the ZARU on the INS output data. This allows the EKF to correct the velocity error and angular rate bias after each stride, breaking the cubic-in-time error growth of the position and replacing it with an error accumulation that is linear in the number of steps, see Figure 3.1 and Figure 3.2 [3, 4, 5, 6].

In the first section a basic concept of walking event is given, followed by an analysis of step detection techniques used in the thesis. To understand how the walking event can be detected two methods were analyzed, squared Euclidean norm of the acceleration and variance of the squared Euclidean norm.

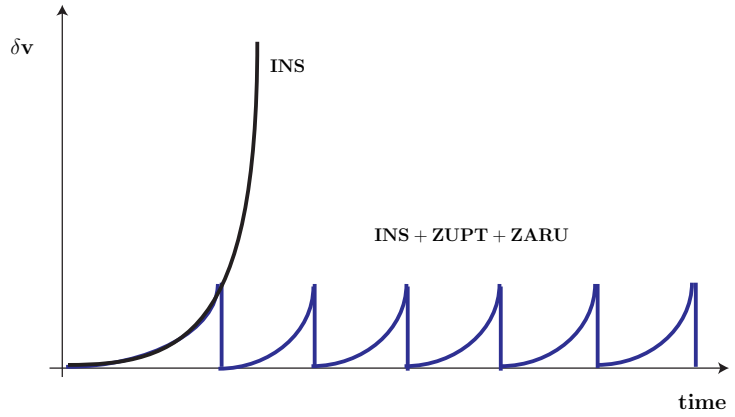

Figure 3.1: *The error growth in velocity. The black curve represents the INS estimates only and the blue curve is a plot of INS with aid of ZUPT and ZARU. The error is immediately zero when the stance phase is detected.*

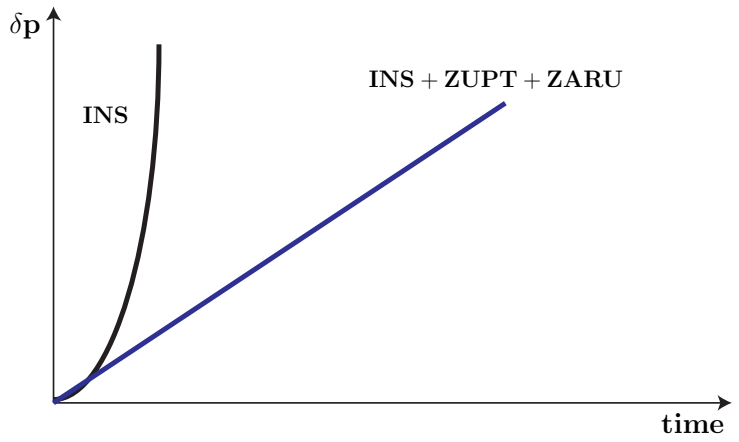

Figure 3.2: *The error growth in position. The black curve represents the INS estimates only and the blue curve is a plot of INS with aid of ZUPT and ZARU.*

3.1 Walking event

When walking, the gait cycle begins just after the foot strikes the ground, usually with heels first, causing a large peak acceleration followed by an oscillation, see Figure 3.3. The foot remains stationary for approximately 0.5 s. During the stance phase the accelerometer measures the earth gravitational acceleration. The velocity and angular rates are zero. The initial swing phase starts when the opposite foot strike event starts [5]. In order to apply the ZUPT and ZARU it is not necessarily need an identification of the exact onset and end of a footfall. Rather, it is sufficient to identify a single instance time within the foot is resting on the ground, during which all accelerations, angular rates and velocities are zero. In practice, this is not trivial, because the accelerometers suffer from drift, so they never show exactly zero [4].

Different methods can be used to detect a walking event based on an accelerometer signal, including the approaches based on analysis of magnitude of signal, signal crossing the gravity value and signal variance based approaches. Following subsection gives a description of IMU measurements during a walking event.

3.1.1 IMU measurements

The acceleration measurements from the IMU at time k can be written as

is the gyro bias, $\delta\mathbf{r}$ is the position error, $\delta\mathbf{v}$ represents the velocity error and the $\delta\mathbf{a}$

$$\widetilde{\mathbf{a}}_k = \mathbf{a}_k + \delta\mathbf{a} + \mathbf{e}_{k,a} \tag{3.1}$$

where $\widetilde{\mathbf{a}}_k$ is the output of the IMU and $\mathbf{a}_k$ is the real acceleration, $\delta\mathbf{a}$ is the bias, which is constant and $\mathbf{e}_{k,a}$ is a Gaussian noise, $\mathbf{e}_{k,a} \sim \mathrm{N}(0,\sigma_a)$. The same model can be applied the angular rates measurement.

$$\widetilde{\omega}_k = \omega_k + \delta\omega + \mathbf{e}_{k,\omega} \tag{3.2}$$

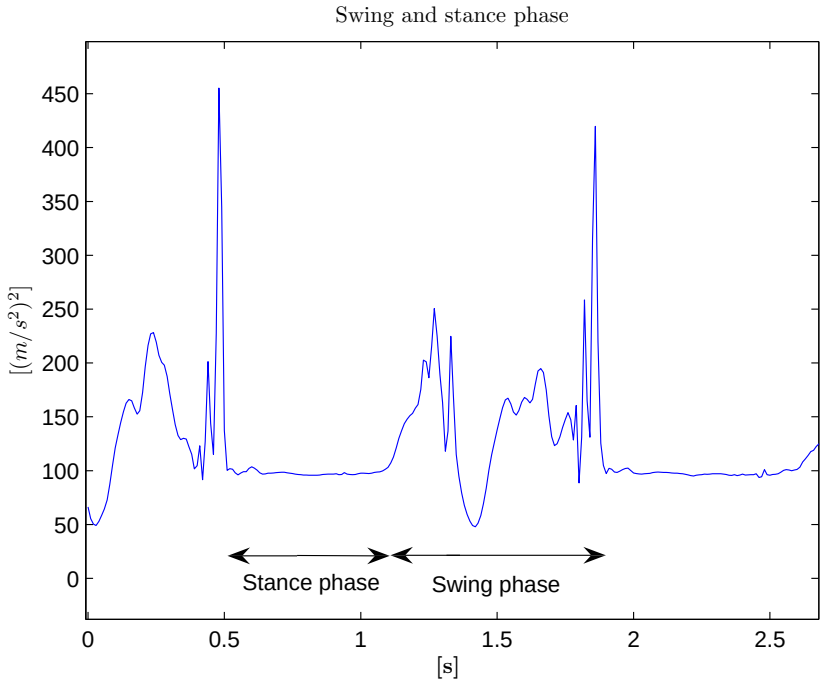

Figure 3.3: *This figure shows the norm squared of a walking foot. The black arrow shows the stance, respective stride phase's duration.*

$\widetilde{\omega}_k$ is the output of the IMU, ω_k is the real angular rates, $\delta\omega$ is the bias and $\mathbf{e}_{k,\omega}$ is a normally distributed noise, $\mathbf{e}_{k,\omega} \sim \mathrm{N}(0,\sigma_\omega)$. The biases are not really constants, but in the project they are treated as constants.

3.2 Squared norm analysis

During the stance phase the accelerometer should only measure the gravitational acceleration and the angular rate, ω_k, is equal to zero. Taking the squared Euclidean norm of the acceleration yields

$$\|\widetilde{a}_{k,x} + \widetilde{a}_{k,y} + \widetilde{a}_{k,z}\|^2 \tag{3.3}$$

where $\widetilde{a}_{k,i}$, i=x,y,z is the acceleration output of the IMU in three different axes. Equation 3.3 can be altered to include several stationary properties of the system. During stance phase, the only acceleration is the gravitational acceleration. From the properties of the normal distribution it is known that if $\widetilde{a}_{k,i}$ is normally distributed then 3.3 corresponds to

$$\|\widetilde{a}_{k,x} + \widetilde{a}_{k,y} + \widetilde{a}_{k,z}\|^2 \sim \chi^2_3(g^2) \tag{3.4}$$

Another statical property is that the sum of χ^2_3 variables is normally distributed in the limit. Plotting the distribution function against a normal distribution, it can be seen that the squared norm is close to a normal distribution, as displayed by Figure 3.4.

The simplest form of event detection is to test when the signal exceeds a threshold value. For example, it can be assumed that if the last five samples have a value close to $1[g^2]$, then it must be a stance phase. Similarly, if the goal is to detect foot strike events, the squared norm values must be greater then $1[g^2]$. Since the χ^2_3 distribution, detailed in equation 3.4, has almost similar size of tail on each side on its distribution function, see Figure 3.5, a confidence interval is taken as shown in equation 3.5. The α in equation 3.5 is the confidence grade. Since it is not necessary to detect the entire time of the swinging phase the α was set to 50 % which corresponds to [85, 110].

$$\chi^2_{3,1-\alpha/2}(g^2) < \|\widetilde{a}_{k,x} + \widetilde{a}_{k,y} + \widetilde{a}_{k,z}\|^2 < \chi^2_{3,\alpha/2}(g^2) \tag{3.5}$$

3.3 Variance analysis

Variance was observed from a sliding window, [11]. The variance, s^2_n, of n data samples is

$$s^2_n(x_i) = \frac{1}{n}\sum_{i=1}^{i=j+n}(x_i - \overline{x}_j)^2 \tag{3.6}$$

where $\overline{x}_j$ is the mean of n samples. Properly applied, the variance of the squared norm can be useful for detecting gait events where the signal changes suddenly, such as a heel strike and the stance phase initiation, [5]. If the variance of a manipulated signal is to be used for gait event detection, the sample size n must be chosen appropriately so that the variance test is adequately sensitive to slow signal changes and adequately responsive to fast ones. It was found that a sample size of five to ten was suitable for a gait event. In Figure 3.5, the sample size was set to 5.

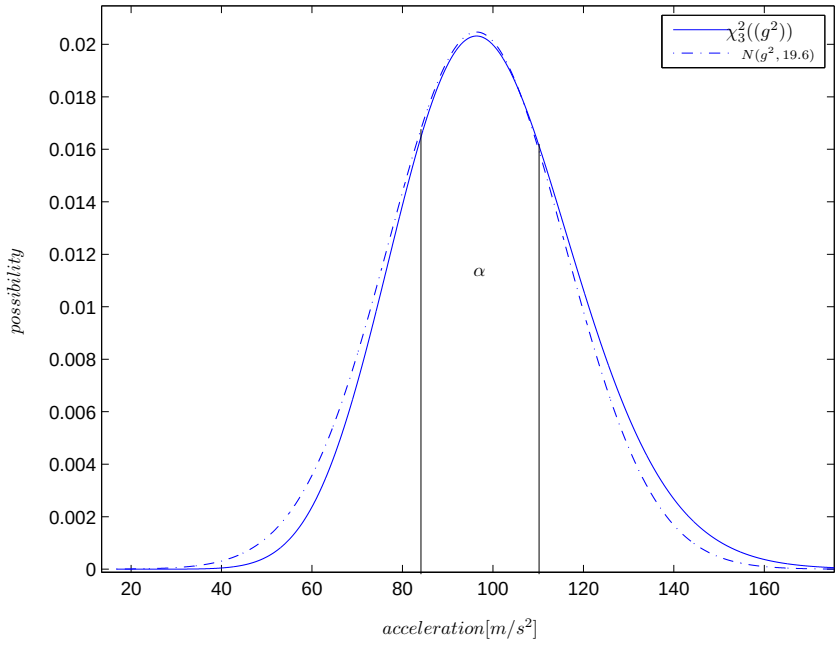

Figure 3.4: *The figure shows the distribution function of the normal distribution* $N(g^2, \sigma)$ *and the distribution function of* $\chi^2_3(g^2)$*. The straight line on the figure shows the threshold values used for determine if the sample belongs to stance phase.*

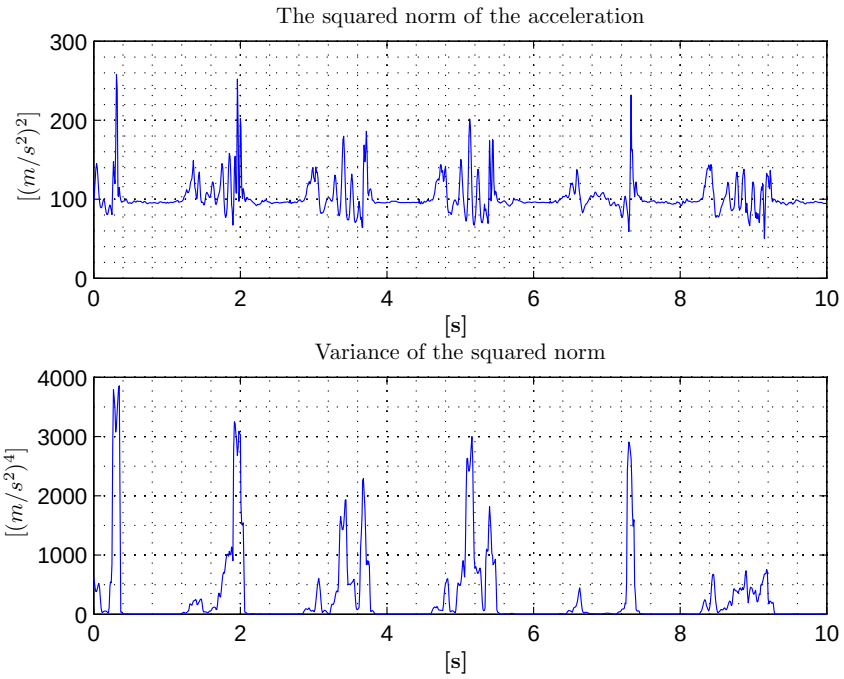

Figure 3.5: *First plot shows the squared norm and the second plot shows the variance.*

3.4 The detector

The squared Euclidean norm method gives a good approximation, but there are some limitations. When the foot has no acceleration, when it is in the linear motion, the squared norm method is unstable. The squared Euclidian norm provides a fluctuating curve and it will not always be correct to detect the stance phase with a predetermined threshold value, which means that there are samples which can be detected, event if the samples do not belong to the stance phase. The variance method is an averaged approximation and the sample size is a sensitive variable in the method. Since it is an averaged approximation, there are possibilities to detect smaller stance phase duration. Foot in linear motion is also another fact that makes the variance method unstable. In order to disregard the issue about the foot in the linear motion, the angular rate measurements were used. Angular rate is zero, when the foot is in the stance phase, but it can also be zero in the swinging phase when shifting the angles from minus to plus.

The detector which is introduced in the thesis uses the both methods with the angular rate measurements. It has a simple design using three requirements. First requirement is that the measured squared Euclidean norm of the acceleration should be inside the predetermined threshold values. Secondly, the angular rate should be close to zero and thirdly the variance should be limited during the stance phase. These three requirements results in that all sample k which fulfills equations 3.7, 3.8 and 3.9 belongs to the stance phase. The result can be seen in Figure 3.6, 3.7 and 3.8

$$(\|\widetilde{a}_{k,x} + \widetilde{a}_{k,y} + \widetilde{a}_{k,z}\|^2) \in [85, 110][(m/s^2)^2] \tag{3.7}$$

$$s_n^2(\|\widetilde{a}_{k,x} + \widetilde{a}_{k,y} + \widetilde{a}_{k,z}\|^2) < 20 \tag{3.8}$$

$$-18^o < \widetilde{\omega}_i, k < 18^o \tag{3.9}$$

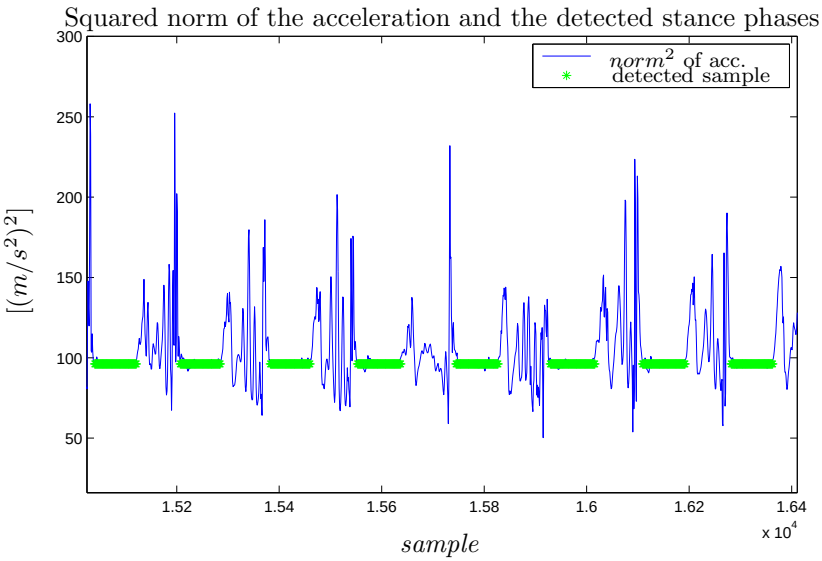

Figure 3.6: *This figure shows the detected stance phases with a plot of the squared norm of the acceleration.*

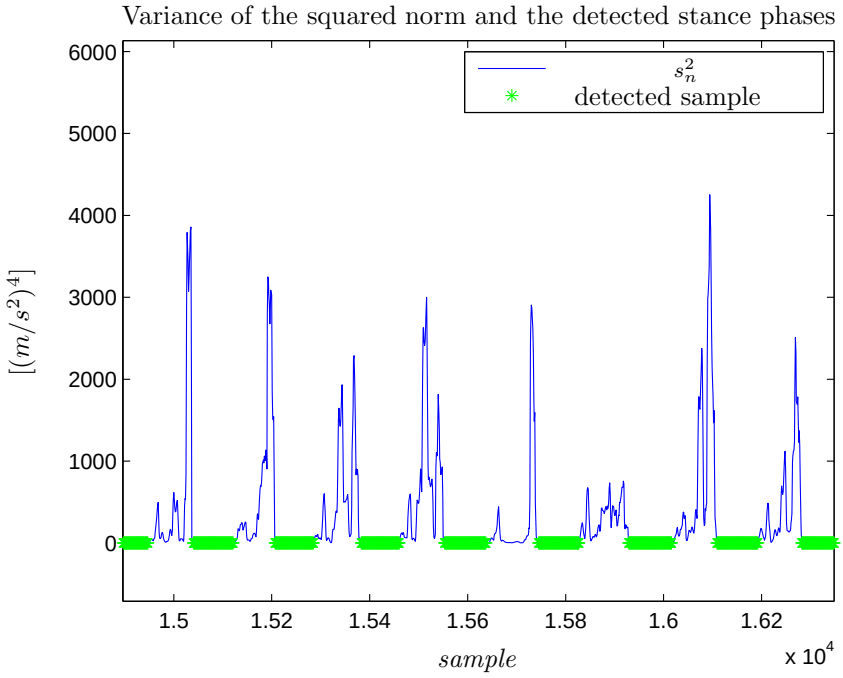

Figure 3.7: *This figure shows the detected stance phases with a plot of the variance.*

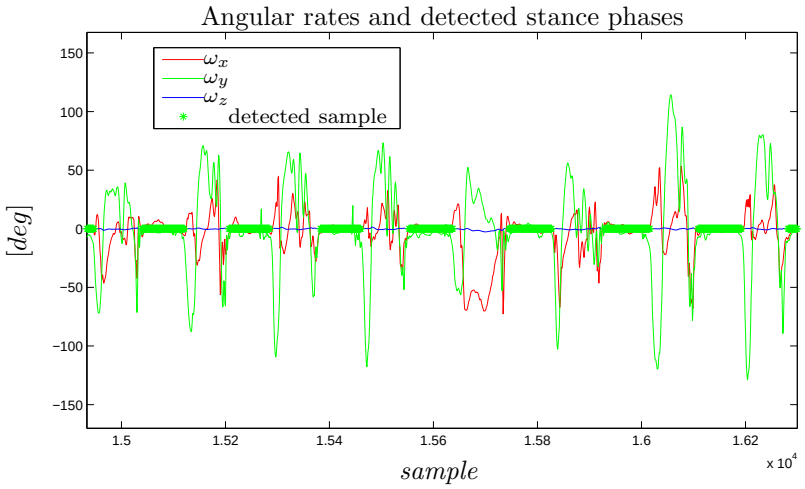

Figure 3.8: This figure shows the detected stance phase with a plot the angular rates.

Chapter 4

Integration of the system

In this chapter a method for combining the inertial navigation system (INS) data with the zero velocity update (ZUPT) and the zero angular rate update (ZARU) techniques is described. The method uses the Extended Kalman Filter (EKF) which is the intelligent signal processing algorithm used in the thesis. The INS provides the EKF with the position, the velocity and the attitude. The detector gives information whether it is the stance phase or the swing phase and let the EKF filter composite the measurement matrix. The measurement matrix is a non zero matrix only if it is a stance phase and when the masurement matrix is properly initialized, the ZUPT and ZARU are introduced. The EKF estimates the INS error based on the output of the INS and the step detector. The error vector from the EKF is then used to correct the INS internal state, see Figure 1.1. At the next measurement epoch, the INS again produces the total navigation-state estimate to EKF and the detector decides whether to apply ZUPT and ZARU techniques.

In the first section the usual kalman filter is introduced and in the next section the EKF filter used in the thesis is presented.

4.1 The Kalman Filter

The Kalman filter has been introduced in the early 1960's and since then found widespread use. One important area of use for Kalman filtering is inertial navigation systems. The signal model is

$$\mathbf{x}_{k+1} = \mathbf{\Phi}_k \mathbf{x}_k + \mathbf{G}_k \mathbf{w}_k \tag{4.1}$$

$$\mathbf{y}_k = \mathbf{H}\mathbf{x}_k + \mathbf{n}_k \tag{4.2}$$

where the $\dim(\mathbf{x}_k) = m$ and the $\dim(\mathbf{y}_k) = p$. $\mathbf{\Phi}$ is the state transition matrix and $\mathbf{H}$ is the measurement matrix. The process $\mathbf{w}_k$ is the measurement noise and $\mathbf{n}_k$ is the process noise, both are zero mean white noise with

$$E[\mathbf{w}_l \mathbf{w}_m^T)] = \mathbf{Q}\delta(l-m) \tag{4.3}$$

$$E[\mathbf{n}_l \mathbf{n}_m^T] = \mathbf{R}\delta(l-m) \tag{4.4}$$

4.1.1 Notations

The notations used to describe the Kalman filter is

- $\hat{\mathbf{x}}_k$ is the estimation of $\mathbf{x}_k$.
- $\mathbf{P}_k = E[\delta\mathbf{x}_k \delta\mathbf{x}_k^T]$, where $\delta\mathbf{x}_k = \mathbf{x}_k - \hat{\mathbf{x}}_k$
- $\hat{\mathbf{x}}_{k+1}^-$ is the state prediction error.
- $\hat{\mathbf{y}}_{k+1}^-$ is the linear least square estimator of $\mathbf{y}_k$
- $\mathbf{P}_k^- = E[\delta\mathbf{x}_k^- \delta\mathbf{x}^{-T}_k]$
- $\mathbf{\Phi}_k$ is the state transition matrix.
- $\mathbf{H}_k$ is the measurement matrix.
- $\mathbf{K}_{f,k}$ is the Kalman gain.

The Kalman filter has two distinct phases' time update and measurement update. The time update phase uses the state estimate from the previous time step to produce an estimate of the state at the current time step. In the measurement update phase, measurement information at the current time step is used to refine this time updated state to arrive at a new, more accurate state estimate, again for the current time step. Below a table is shown of the Kalman filter.

Time update.
$\hat{\mathbf{x}}_{k+1}^- = \mathbf{\Phi}_k \, \hat{\mathbf{x}}_k$
$\hat{\mathbf{y}}_{k+1}^- = \mathbf{H}_k \, \hat{\mathbf{x}}_{k+1}^-$
$\mathbf{P}_{k+1}^- = \mathbf{\Phi}_k \, \mathbf{P}_k \, \mathbf{\Phi}_k^* + \mathbf{G}_k \, \mathbf{Q}_k \, \mathbf{G}_k^*$
Measurement update.
$\mathbf{K}_{f,k} = \mathbf{P}_k^- \, \mathbf{H}_k^* \, (\mathbf{H}_k \, \mathbf{P}_k^- \, \mathbf{H}_k^* + \mathbf{R}_k)^{-1}$
$\hat{\mathbf{x}}_k = \hat{\mathbf{x}}_k^- + \mathbf{K}_{f,k} \, (\mathbf{y}_k - \mathbf{H}_k \, \hat{\mathbf{x}}_k^-)$
$\mathbf{P}_k = \mathbf{P}_k^- - \mathbf{K}_{f,k} \, \mathbf{H}_k \, \mathbf{P}_k^-$

Table 4.1: *The Kalman filter recursions in time and measurement update form [13].*

4.2 The Extend Kalman Filter

In the extended Kalman filter, (EKF) the state transition and observation models need not be linear functions of the state but may instead be differentiable functions.

$$\mathbf{x}_{k+1} = \mathbf{f}_k(\mathbf{x}_k) + \mathbf{w}_k \tag{4.5}$$

$$\mathbf{y}_k = \mathbf{h}(\mathbf{x}_k) + \mathbf{n}_k \tag{4.6}$$

The function $\mathbf{f}_k(\mathbf{x}_k)$ can be used to compute the predicted state from the previous estimate and similarly the function $\mathbf{h}(\mathbf{x}_k)$ can be used to compute the predicted measurement from the predicted state. However, $\mathbf{f}_k(\mathbf{x}_k)$ and $\mathbf{h}(\mathbf{x}_k)$ cannot be applied to the covariance directly. Instead a matrix of partial derivatives (the Jacobian) is computed. At each time step the Jacobian is evaluated with current predicted states. These matrices can be used in the Kalman filter equations. This process essentially linearizes the non-linear function around the current estimate [13]. Consider the linearized error state $\delta\mathbf{x} = \widehat{\mathbf{x}} - \mathbf{x}$, where $\widehat{\mathbf{x}}$ is the estimated states and $\mathbf{x}$ is the true state. The error state contains

$$\delta\mathbf{x} = \begin{bmatrix} (\phi^T & \delta\omega^T & \delta\mathbf{r}^T & \delta\mathbf{v}^T & \delta\mathbf{a}) \end{bmatrix}^T \tag{4.7}$$

where ϕ is the attitude error, $\delta\omega$ is the gyro bias, $\delta\mathbf{r}$ is the position error, $\delta\mathbf{v}$ represents the velocity error and the $\delta\mathbf{a}$ represents the accelerometer bias. The EKF filter delivers the error estimated after each estimation cycle to the INS. At that time, the INS sets the acceleration and angular rates to zero. The navigation system's linearized error model is

$$\delta\mathbf{x}_k = \mathbf{\Phi}_{k-1}\delta\mathbf{x}_{k-1} + \mathbf{w}_{k-1} \tag{4.8}$$

where $\mathbf{w}_k$ is considered as a zero mean white noise with covariance matrix

$$\mathbf{Q}_k = E(\mathbf{w}_k\mathbf{w}_k^T) \tag{4.9}$$

The measurement is

$$\mathbf{z}_k = \mathbf{H}\delta\mathbf{x}_k + \mathbf{n}_k \tag{4.10}$$

where $\mathbf{n}_k$ is measurement noise which is considered to be zero-mean white gaussian noise with covariance matrix

$$\mathbf{R}_k = E(\mathbf{n}_k\mathbf{n}_k^T) \tag{4.11}$$

The state transition matrix for the discrete time dynamics in the EKF is

$$\mathbf{\Phi} = \begin{bmatrix} \mathbf{I} & -\Delta T\mathbf{R}_{b2t} & 0 & 0 & 0 \\ 0 & \mathbf{I} & 0 & 0 & 0 \\ 0 & 0 & \mathbf{I} & \Delta T\mathbf{I} & 0 \\ \Delta T\mathbf{S}(\mathbf{f}^t) & 0 & 0 & \mathbf{I} & -\Delta T\mathbf{R}_{b2t} \\ 0 & 0 & 0 & 0 & \mathbf{I} \end{bmatrix} \tag{4.12}$$

and $\mathbf{R}_{b2t}$ is the rotation matrix that transforms vectors from the b-frame to the t-frame. This is presented in the matrix subblocks $(1,2)$ and $(4,5)$ in the equation(4.12) since the gyro and accelerometer biases are represented in the body frame. In the matrix subblock $(1,4)$, the expression $\mathbf{S}(\mathbf{f})^t$ is the skew-symmetric cross-product operator matrix,

$$\mathbf{S}(\mathbf{f}^t) = \begin{bmatrix} 0 & -f_z & f_y \\ f_z & 0 & -f_x \\ -f_y & f_x & 0 \end{bmatrix} \tag{4.13}$$

and the $\mathbf{f}^t$ vector is formed from the t-frame accelerometer output vector as

$$\mathbf{f}^t = \mathbf{R}_{b2t}\mathbf{f}^b \tag{4.14}$$

With the table 4.1 it is now clearly seen how the EKF works on the inertial navigation system. It is known that

$\mathbf{Q}_k/\mathbf{R}_k$ small $\Rightarrow$ good tracking, but noise sensitive.
$\mathbf{Q}_k/\mathbf{R}_k$ large $\Rightarrow$ bad tracking, but less noise sensitive.

4.3 The observation model during the stance phase

ZUPT and ZARU techniques are applied in the EKF, if the detector decides that the foot is stationary. When the foot is at stance phase, the measuremnt is performed on velocity error and angular rate bias. The $\mathbf{z}$ vector in equation 4.10 is a zero vector in the swing phase and in the stance phase it is given by

$$\mathbf{z} = \begin{pmatrix} \delta\omega \\ \delta\mathbf{v} \end{pmatrix} \tag{4.15}$$

The measurement sensitive matrix is a zero matrix in the swing phase and in the stance phase it is given by

$$\mathbf{H} = \begin{pmatrix} 0 & \mathbf{I} & 0 & 0 & 0 \\ 0 & 0 & 0 & \mathbf{I} & 0 \end{pmatrix} \tag{4.16}$$

The $\mathbf{H}$ matrix selects the velocity error component and the angular rate component from the error state vector $\delta\mathbf{x}$. This allows EKF to apply ZUPT and ZARU. The covariance matrix $\mathbf{R}$ should be close to zero, during the stance phase.

Chapter 5

Hardware

This chapter includes a short description of the hardware used in the thesis. The hardware consists of two distinguishable parts. Firstly, the IMU which consist of three gyros, measuring the angular rates in three dimension and tree accelerometers, which measure the acceleration in three dimension. Secondly, a PC where the proposed integration of algorithm is implemented.

5.1 The Inertial Measurement Unit

The inertial measurement unit comprises three gyros and three accelerometers. The sensor is mounted on the foot. The sensor communicates with the host PC using the USB port. The sampling rate of the sensor data is 100 Hz. The accelerometers and the gyroscope measure the accelerations and the angular rate in the body frame coordinates. To finally obtain the result in the tangent-frame, a coordinate transformation from the body's to the tangent's coordinate frame has to be processed.

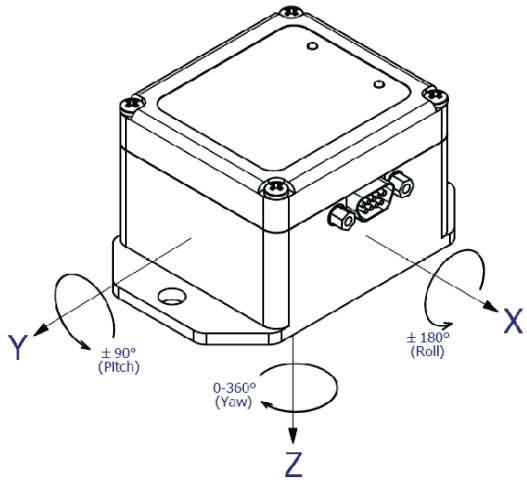

Figure 5.1: *The IMU used in the project.*

Chapter 6

Results

In this chapter the results of the project are presented. The system which was built during the project was tested with real world data as well as simulated data. The first subsection herein will contain the results from simulated data, whereas the results from real world data will come in the second subsection.

6.1 Results from the simulated data

To test the integration strategy, a simulation of the walk scenario was performed. The simulated data that of a user walking on a trajectory, where the ω_x and $\omega_{y,}$ are initialized to be a zero vector. The ω_z vector is a non-zero vector, which is initialized to be 30^o for a half second after ten seconds, 50^o for a half second after forty seconds, -30^o for a half second after hundred seconds and -50^o for a half second after hundred fifty seconds. The gravitational acceleration in z_b-axis was added. The forward acceleration in x_b-axis was initialized to be $\pm 2[m/s]$ with intervals with no acceleration. With simulated data there is reference information available that can be used to evaluate the accuracy of the entire trip. The data was simulated for 250[s]. The user is started to walk at the origin in the t-frame.

Figure 6.1 shows the estimated position plotted with respect to the simulated data. Since the position is not directly observable, the trajectory is not very accurate. The position error grows rapidly as the time grows. The highest error is around 15[m] after 220[s]. The walked trajectory length is around $200[m]$ and the walked time is 250[s].

When the foot is stationary, the velocity is fully determinable as displayed in Figure 6.4. When the foot is at swing phase the velocity error can be large, since no states are observable during swing phase. Figure 6.4 can be compared with Figure 3.1.

As discussed earlier in this report we can see that the position error grows linearly to steps taken, see Figure 6.7, which can be compared with Figure 3.2. The bias difference estimate, Figure 6.9, shows that $\widehat{a}_{x,bias}$ and $\widehat{a}_{y,bias}$ are constant and does not converge to zero and gyro biases are fully observable.

In Figure 6.12 the blue line is the real attitude and the dashed red line is the estimated attitude. The yaw heading is not observable. The pitch and roll headings are linearly observable with accelerometer biases. A compromise needs

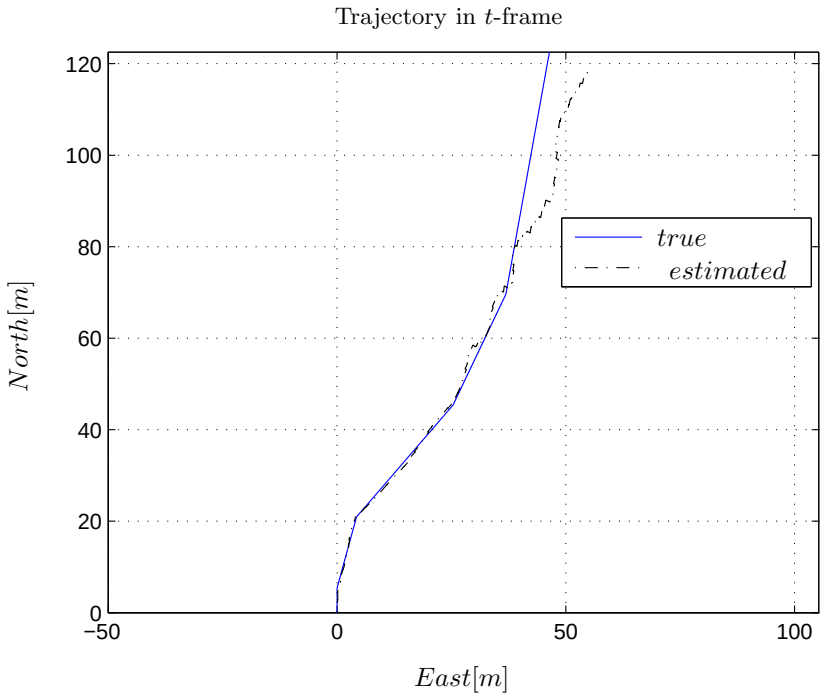

Figure 6.1: *This figure shows the the results from the simulated data. The estimated trajectory is the dashed black line and the true trajectory is the solid blue line.*

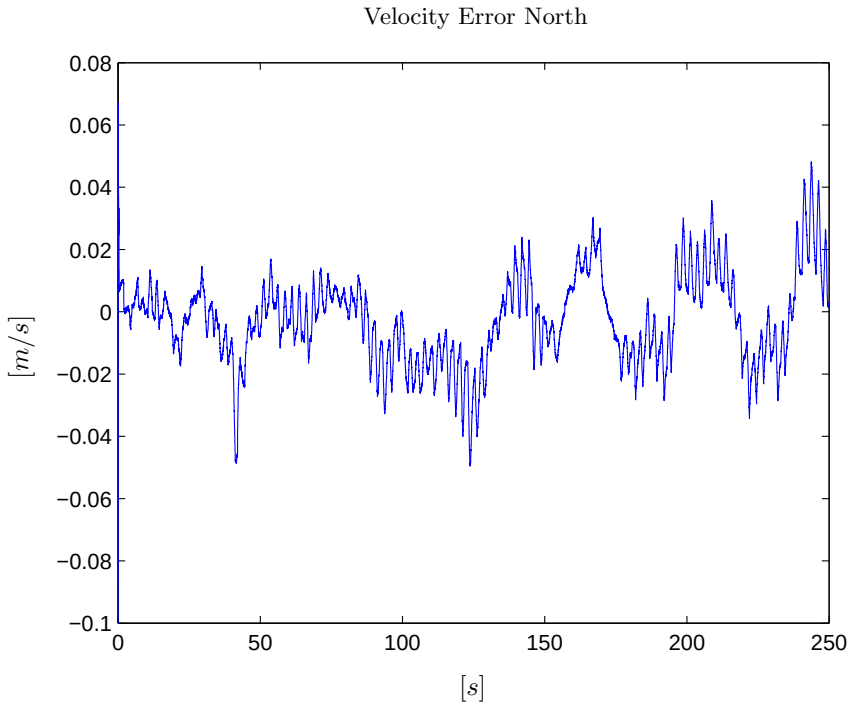

Figure 6.2: *The estimated velocity error in the North direction of the simulated data.*

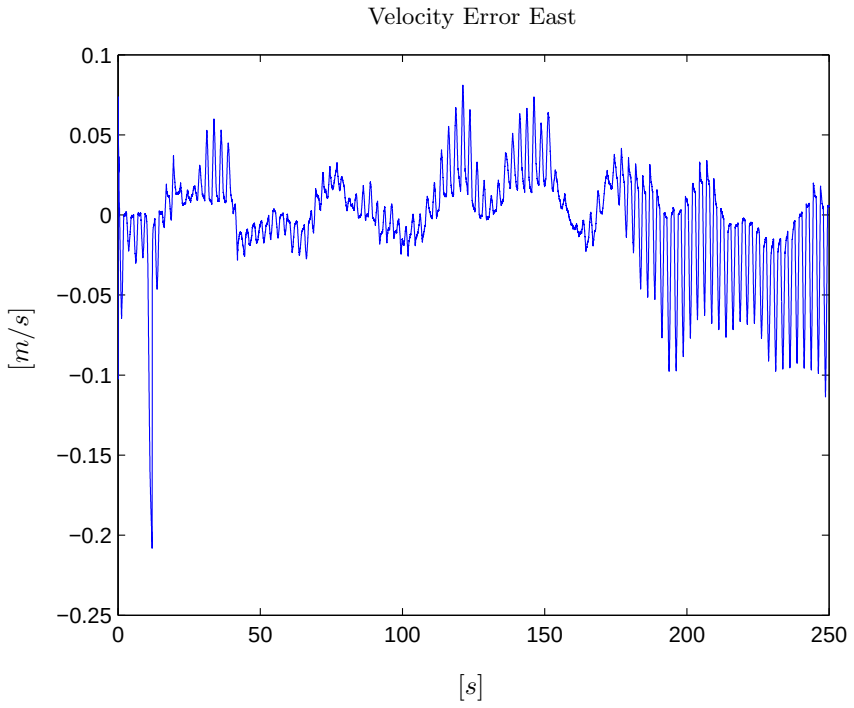

Figure 6.3: *The estimated velocity error in the East direction of the simulated data.*

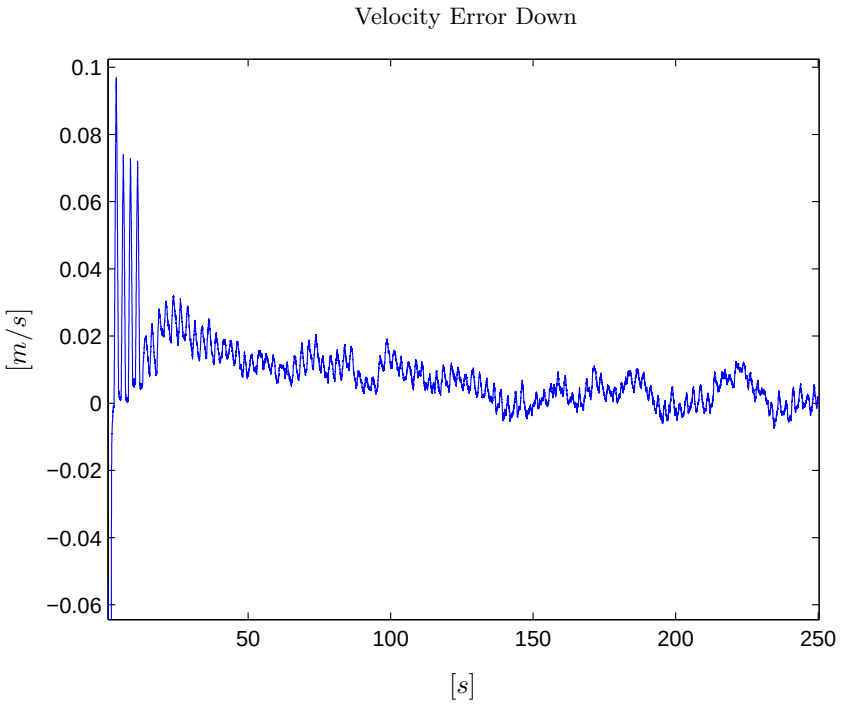

Figure 6.4: *The estimated velocity error in Down direction of the simulated data.*

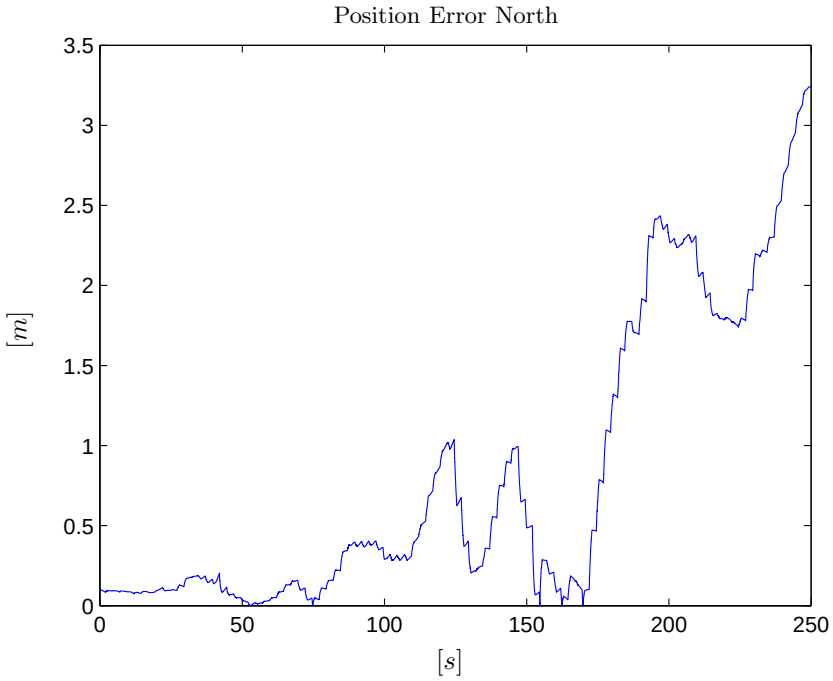

Figure 6.5: *Estimated norm of position error in the North direction.*

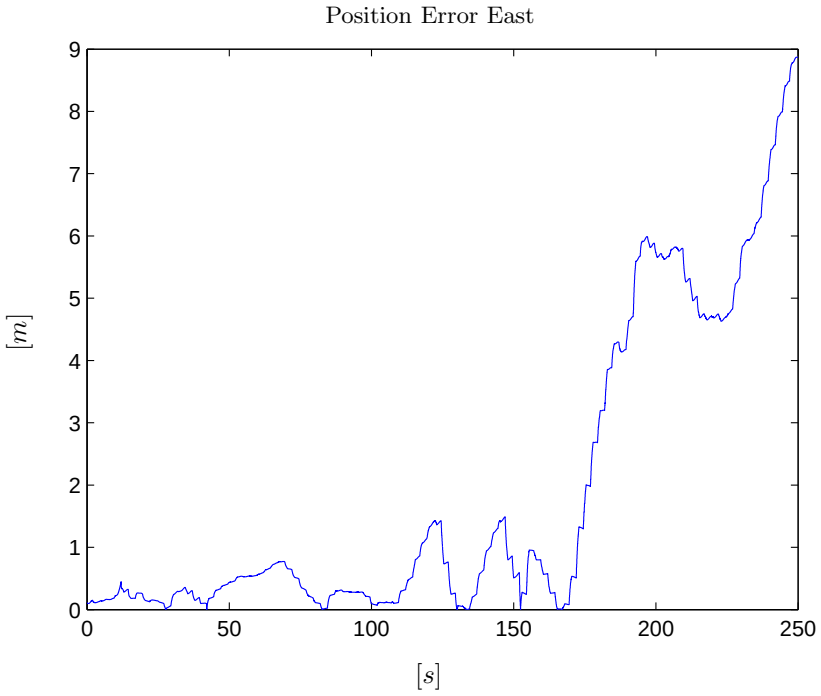

Figure 6.6: *Estimated norm of position error in the East direction.*

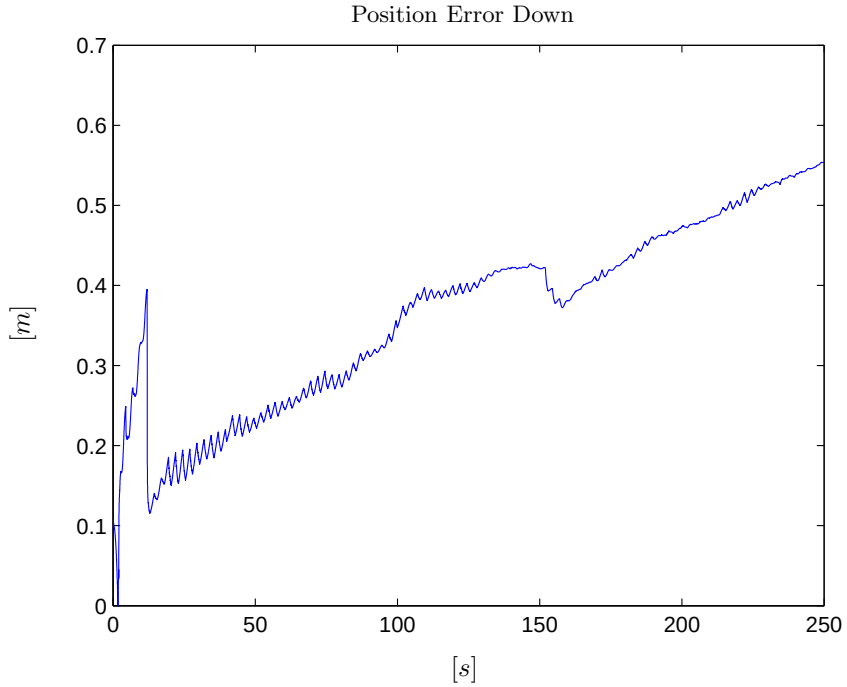

Figure 6.7: *Estimated norm of position error in the Down direction.*

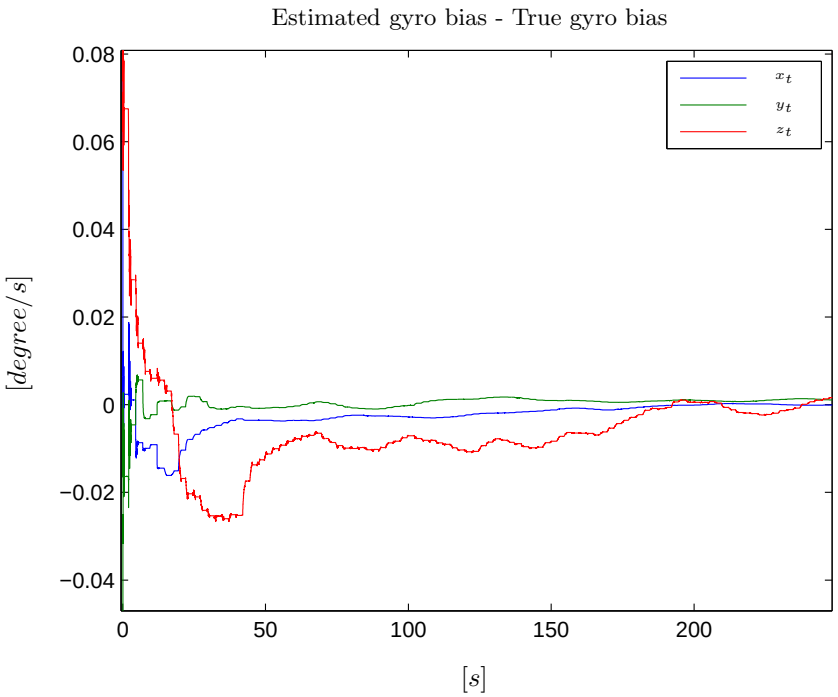

Figure 6.8: *Estimated bias minus true bias of the gyro bias. The blue line is the bias in x_t-axis, the green line is the bias in y_t-axis and the red line is the bias in z_t-axis.*

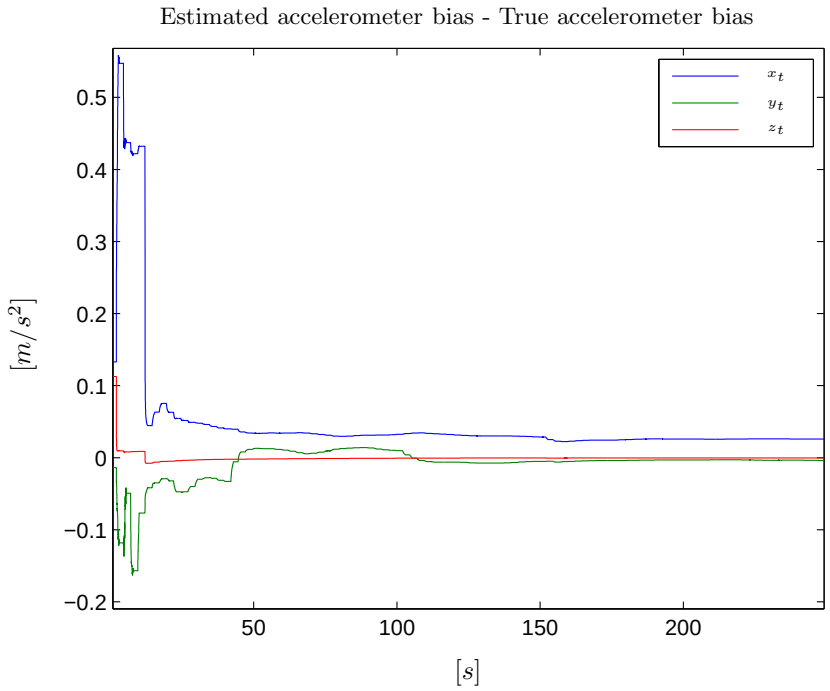

Figure 6.9: *Estimated bias minus true bias of the accelerometer bias. The blue line is the bias in x_t-axis, the green line is the bias in y_t-axis and the red line is the bias in z_t-axis.*

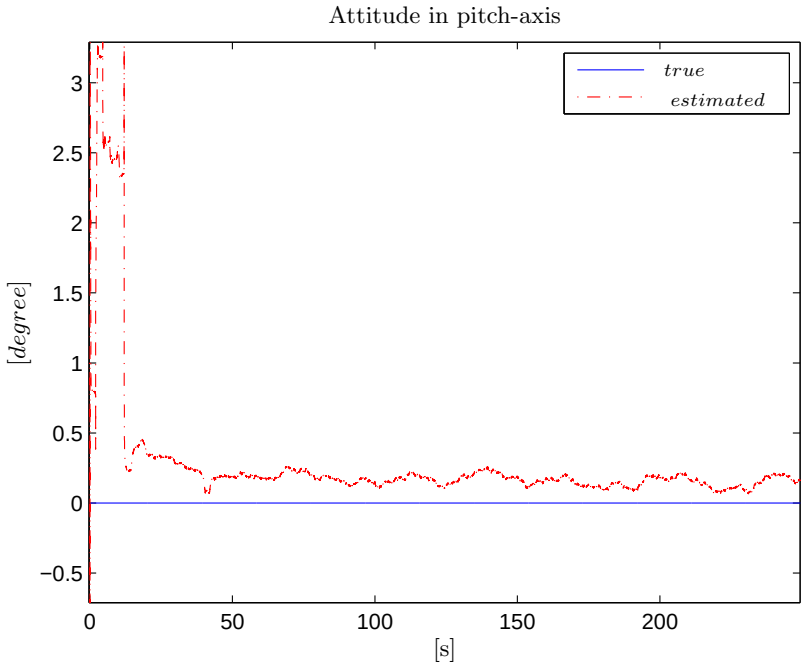

Figure 6.10: *The estimated attitude and the true attitude in the North direction.*

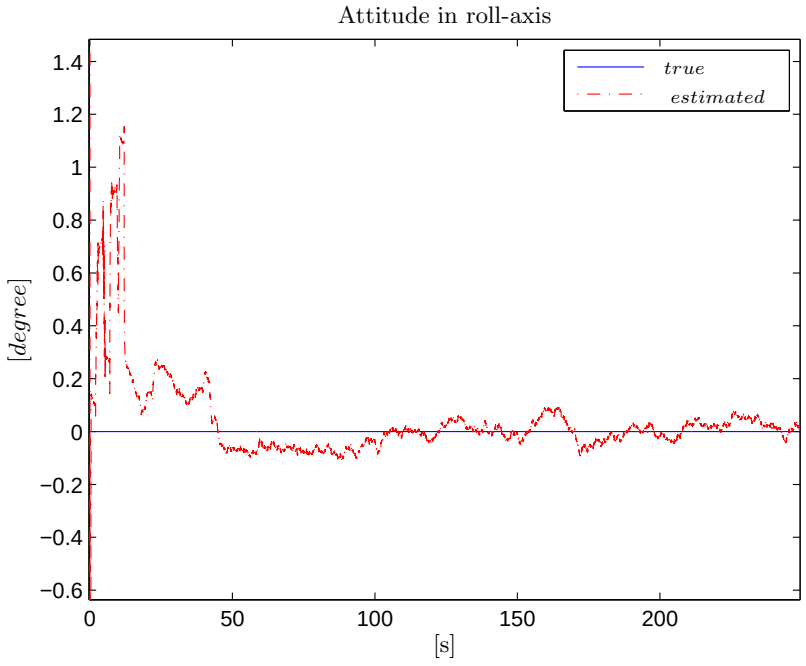

Figure 6.11: *The estimated attitude and the true attitude in the East direction.*

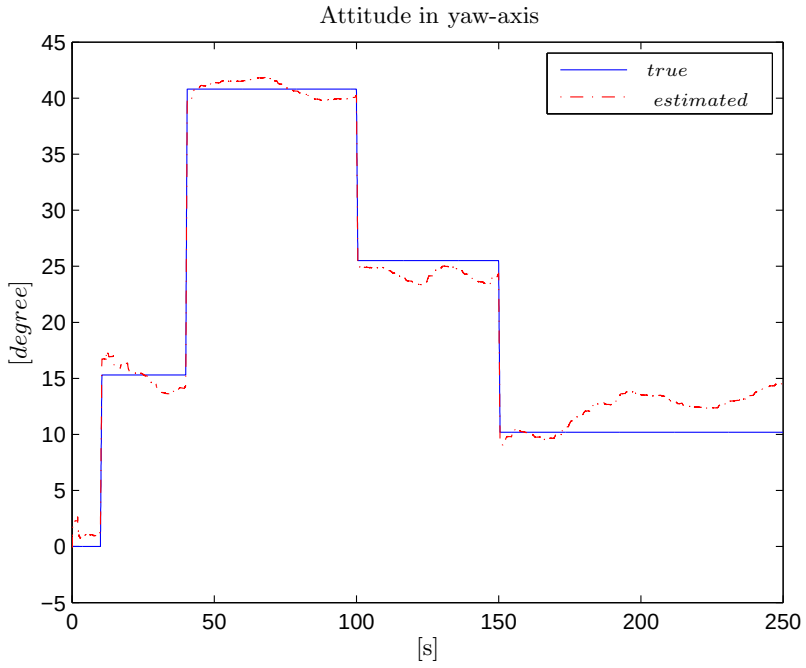

Figure 6.12: *The estimated attitude and the true attitude in the Down direction.*

to be made regarding the accuracy of the variables in the result.

6.2 Results from the real world data

The walking scenario is shown in Figure 6.13. The user was kept stationary for first 120 seconds, whereafter the user walked around a parking space line counterclockwise. The parking line area was roughly 2.5×5[m]. The user started at the position (0, 0, 0) and walked around 45[m] for next 150[s], making a total of three runs around the parking space line. The user ended recording data at position (0, 0, 0). In this test, there was no reference information available except then the parking space line. Figure 6.13 shows the estimated curve of the real world data. The curve is not accurate since the position is not observable. From the Figure 6.13, it may be seen how many steps are taken, 4 steps in the first 2.5[m] and 8 steps in the next 5[m]. There are a variety of aspects that should be taken into account when estimating the trajectory of real data, the velocity of the walking user, the noise variance of IMU and the $\mathbf{R}$ covariance matrix. The $\mathbf{R}$ matrix was the most sensitive variable in the system.

In Figures 6.14 and 6.15 the bias estimates are presented. The bias is constant during the stationary period and oscillate during the swing phase. When the stationary period of the filter is detected the filter resets all velocity component to zero, which can be seen in Figures 6.16, 6.17 and 6.18. The attitude results are good, and we can see the corresponding 90^o turn at each corner on the parking space line.

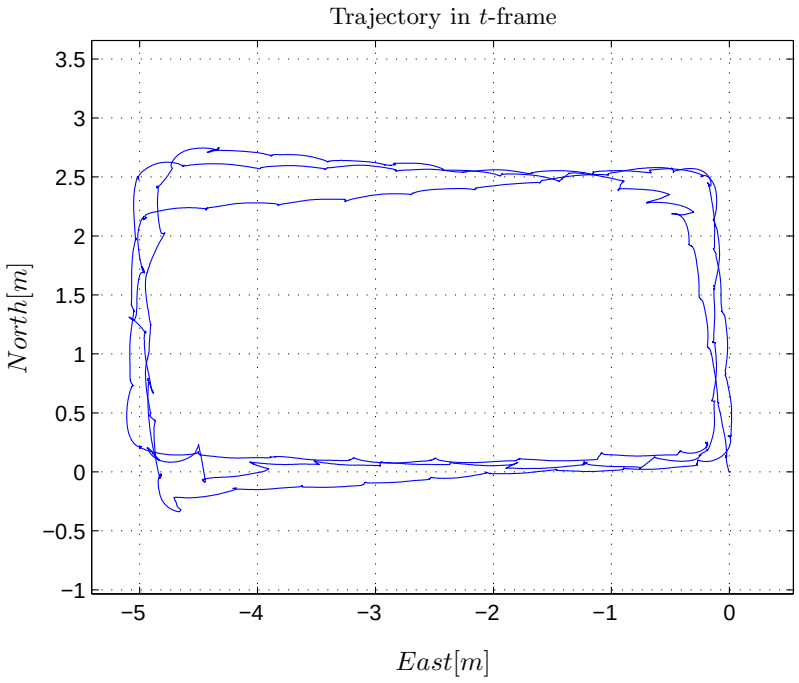

Figure 6.13: *The estimated trajectory. Three runs around the parking space line in 150 s.*

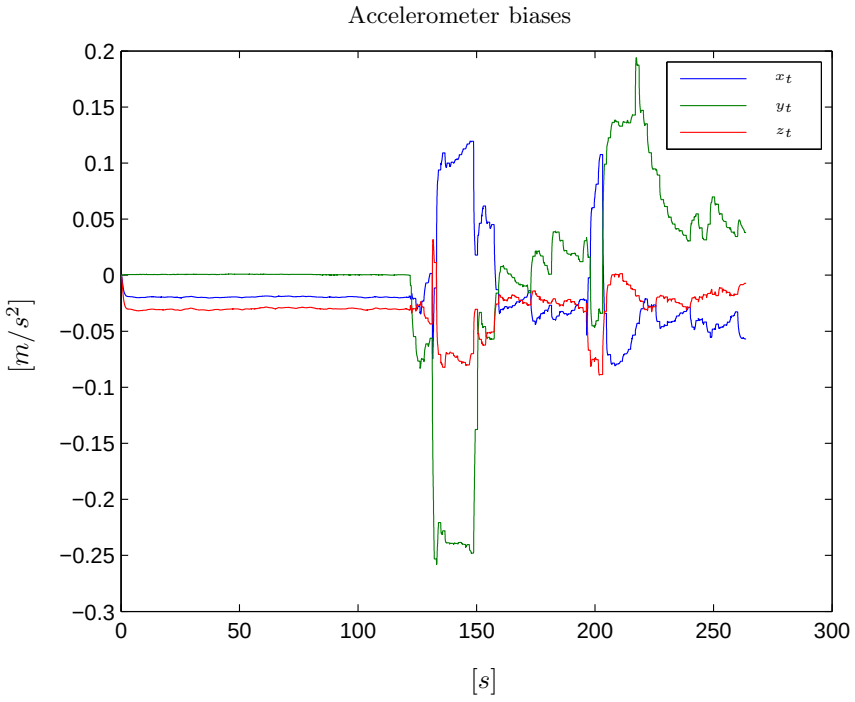

Figure 6.14: *The estimated accelerometer bias. The blue line is the bias in x_t-axis, the green line is the bias in y_t-axis and the red line is the bias in z_t-axis.*

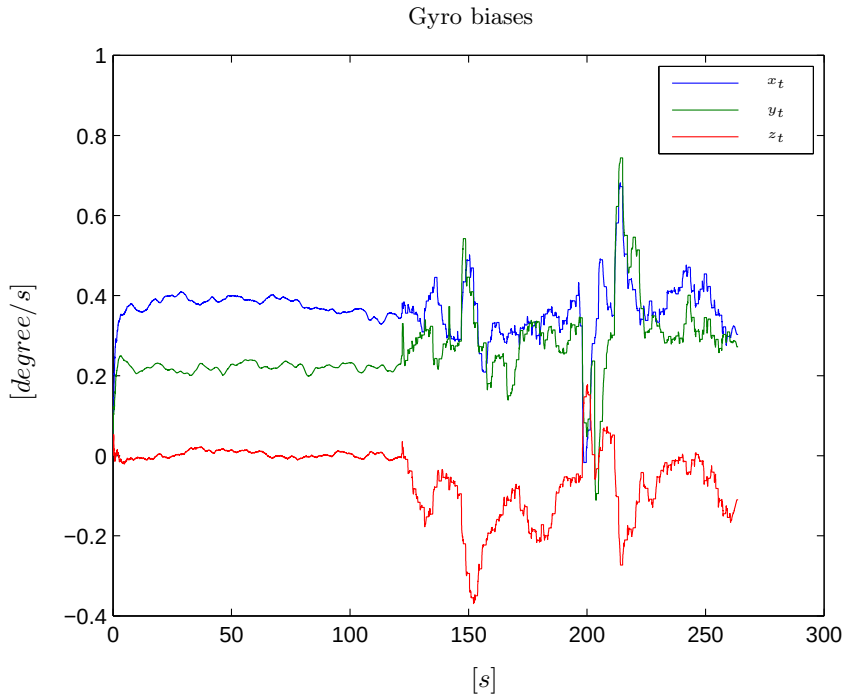

Figure 6.15: *The estimated gyro bias. The blue line is the bias in x_t-axis, the green line is the bias in y_t-axis and the red line is the bias in z_t-axis.*

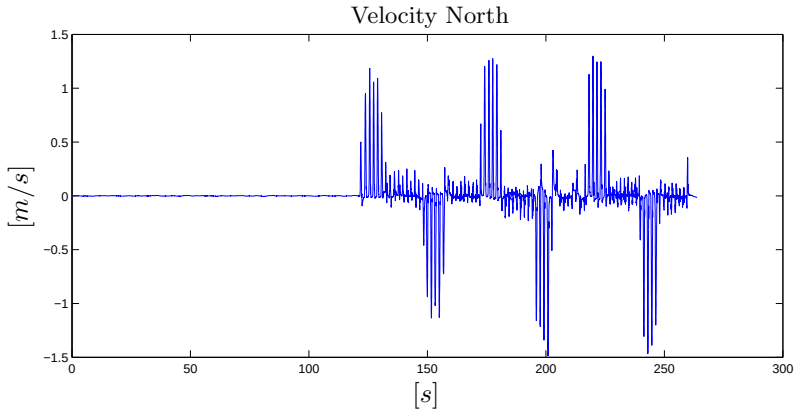

Figure 6.16: *The estimated velocity in the North direction.*

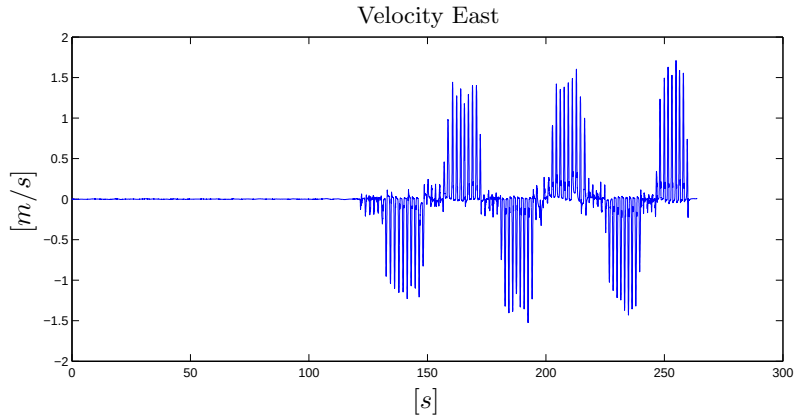

Figure 6.17: *The estimated velocity in the East direction.*

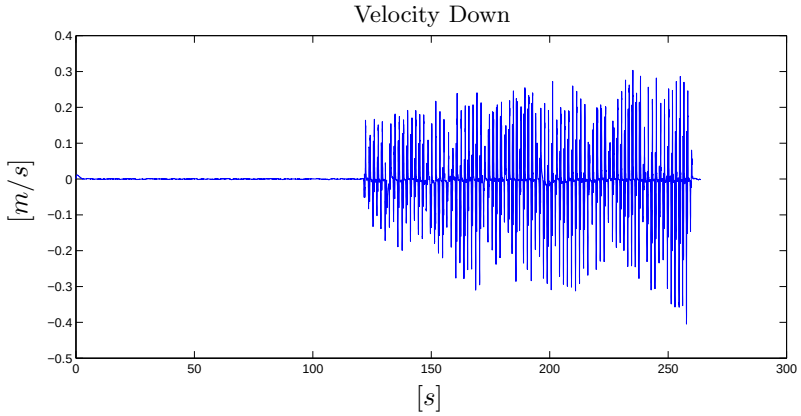

Figure 6.18: *The estimated velocity in the Down direction.*

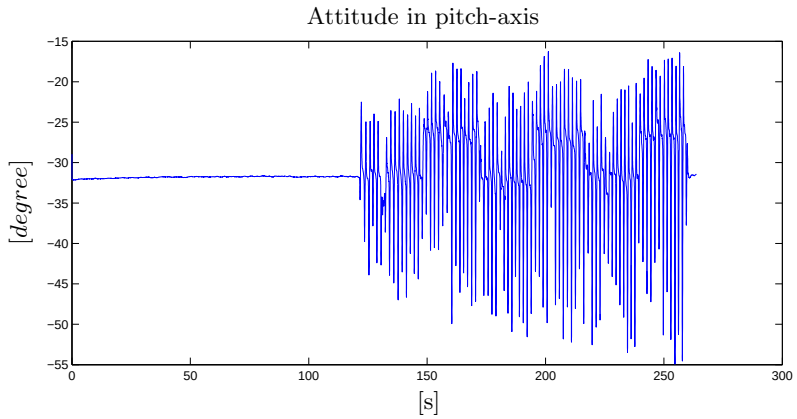

Figure 6.19: *The estimated pitch attitude.*

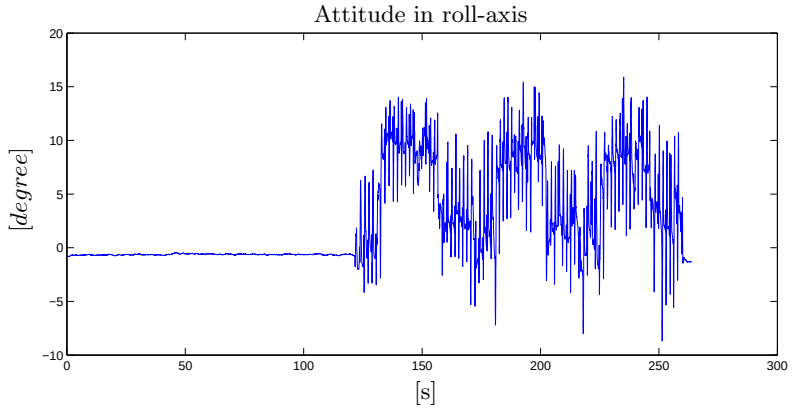

Figure 6.20: *The estimated roll attitude.*

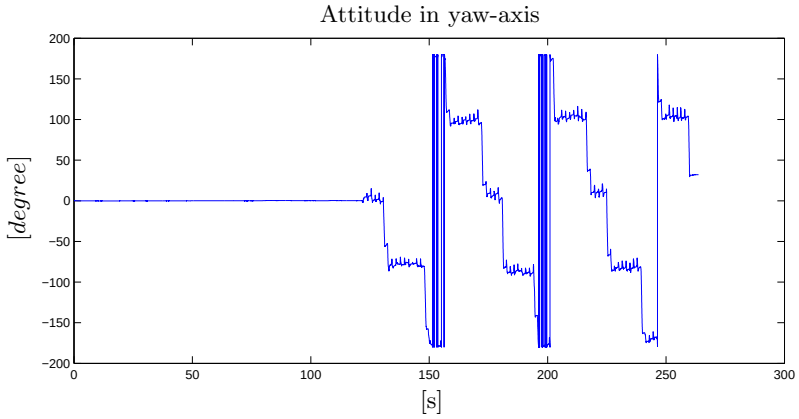

Figure 6.21: *The estimated roll attitude.*

Chapter 7

Conclusions and further work

7.1 Conclusions

The proposed method for indoor navigation for a walking user does work for a short period of time with the aid of ZUPT and ZARU. Another limitation is the velocity of the walk, the implemented system in the thesis works for small velocities around $1 - 2$ $[m/s]$. As mentioned earlier, the output of the system was influenced by a number of parameters, some examples of which are the error covariance matrix $\mathbf{R}$, the initial conditions and the velocity of the user. How the $\mathbf{R}$ matrix was tuned depends on if it was intended for the swinging or the standing phase. If the system is to be used for indoor navigation, it will work better if there is a map of the building accessible. That would enable the position to be observable when the user tries to cross a wall. If the parameters are initialized properly it is clear that the method gives a good approximation to the trajectory.

7.2 Further work

- Integrate the system with a map. Map-correlation techniques can let the user remain indoors longer if the floor plan is known. This could be achieved by simply finding points where the user changes direction and look for features in the floor plan that could constrain where the turns can occur. This information can work in a similar fashion to GPS fix. It is also possible to an extra sensor, like a sonar or optical ranging sensors, to detect the walls. But there is also another method to update the position without having any prior knowledge, simultaneous localization and map-building, which is the SLAM algorithm.

- The detector can be used in other navigation systems where it is necessary to know when the velocity and angular rate bias are zero, for example, in GPS aided INS system. For land vehicles application in urban traffic situations, it is necessary to bound the errors to an acceptable level and the idea is if the vehicle is not moving then apply zero velocity update and

zero angular update integrated with Kalman filter to update error states and covariance.

Bibliography

[1] J. Rantakokko, P. Händel, F. Eklf, B, Boberg, M. Junered, D. Akos, I. Skog, H. Bohlin, F. Neregård, F. Hoffmann, D. Andersson, M. Jansson, P. Stenumgaard, *Positioning of emergency personnel in rescue operations*. Technical report, Royal Institute of Technology, Sweden, Jul. 2007, TRITA-EE 2007:037

[2] J. Farrell and M. Barth, *The Global Positioning System and Inertial Navigation*. New York: McGraw-Hill, 1999.

[3] E. Foxlin, *Pedestrian Tracking with Shoe-monted Inertial Sensors*. Computer Graphics and Applications, IEEE. Volume 25, No. 6. (2005), pp. 38-46.

[4] L. Ojeda and J. Borenstein, *Non-GPS Navigation with the Personal Dead-Reckoning System*. Unmanned Systems Technology IX, Volume 6561, No. 1,2007.

[5] R. Stirling, *Development of a pedestrian navigation system using shoe mounted sensors*. Department of Mechincal Engineering at University of Alberta, 2004, pp. 24-34.

[6] R. Jirawimut, P. Ptanski, V. Garaj, F. Cecelja and W. Balachandran, *A Method for Dead Reckoning Parameter correction in Pedestrian Navigation System*. IEEE Trans. on Instrumentation and Measurement , Vol 52, 2003, No.1, pp. 209-215

[7] J.A. Hesch and S.I. Roumeliotis, *An indoor localization aid for visually impaired*. IEEE Int. Conf. on Robotics and Automation, Roma, Italy, April 10-14, 2007, pp.3545-3551

[8] V. Renaudin, O. Yalak, P. Tome and B. Merminod, *Indoor Navigation of Emergency agents*. European Journal of Navigation, vol. 5, no. 3, pp. 36-45, 2007.

[9] J.T. Kent and T.J. Hainsworth, *Confidence intervals for the noncentral chi-squared distribution*. Journal of Statistical Planning and Inference, Volume 46, Number 2, 1 August 1995, pp. 147-159(13)

[10] A. Lhrke, *GPS-aided Inertial Navigation*. Stockholm: Department of vehicle engineering, Royal Institute of Technology, 2001. pp.6-13 and pp. 21-24.

[11] F. Gusafsson, *Adaptive Filtering and Change Detection*. New York: John Wiley & Sons, 2000, pp. 57-87

[12] M.S. Grewal, L.R. Weill, A.P. Andrews, *Global Positioning System and Inertial Navigation, and Integration*. New York: 2001.

[13] I. Skog, *A low-cost GPS Aided Inertial Navigation System for Vehicular Applications*. Masters thesis, Royal Institute of Technology, Sweden, Mar. 2005, IR-SB-EX-0506